Head Impact Conditions in Simulated Car-to-Bicycle Collisions.

Pablo Lozano, Alessandro Gravina, Yukou Takahashi

Abstract Bicyclist safety remains a critical concern in urban transportation, with current Car-to-Vulnerable Road User (VRU) testing protocols predominantly based on pedestrian impact scenarios. This comprehensive study investigates the biomechanical differences between pedestrian and cyclist collisions across the European context through an integrated approach of accident analysis, Human Body Modelling (HBM) simulation, and statistical modelling. Utilising the Initiative for the Global Harmonization of Accident Data (IGLAD) database, 27 relevant car-bicycle collision cases from 7,055 European accidents were analysed. Employing a M developed in a previous study and four generic vehicle models, simulations were conducted to explore bicyclists' head impact conditions. A statistical surrogate model was developed using Response Surface Models (RSMs) to predict and assess cyclist head impact conditions with computational efficiency. Using the range of car-bicycle impact conditions specifically determined for this study, results showed a mean head impact speed of 42.23 km/h and a head impact angle mean of 50.9 degrees in the windscreen area. RSMs identified the upper hood, windscreen, and roof regions as high-density impact zones for cyclists. Despite various assumptions made for the study, the results obtained give an insight into future considerations of modified test conditions for VRU protection.

Keywords Bicyclist safety, head impact condition, HBM simulation, response surface model.

I. INTRODUCTION

In recent years, there has been a growing recognition of the critical importance of promoting bicycling as a mode of transportation [1-2]. Transportation planning agencies and public health organisations have been increasingly advocating for the integration of bicycling into urban mobility strategies, citing its potential to mitigate the negative impacts associated with automobile use, such as traffic congestion and environmental degradation [3]. This recognition is coupled with a parallel emphasis on enhancing bicyclist safety, particularly in interactions with motor vehicles [4]. This heightened interest stems from an alarming trend of traffic accidents involving bicyclists and vehicles. Analysis of European bicycle accident data reveals that collisions with passenger cars constitute the most significant threat to cyclist fatalities [5].

To address these challenges, researchers and policymakers are increasingly focusing on understanding the factors contributing to bicyclist safety and developing effective strategies to mitigate risks associated with sharing the road with motor vehicles. This includes examining infrastructure designs to separate bicyclists from motor vehicle traffic, enhancing visibility through improved lighting and reflective materials, and promoting protective equipment such as helmets. Moreover, efforts are underway to analyse crash data and identify trends in bicyclist safety to inform evidence-based interventions and policy recommendations. By adopting a comprehensive approach that integrates engineering, education, and enforcement measures, stakeholders aim to create safer roadways for bicyclists and reduce the incidence of traffic accidents involving cyclists and motor vehicles.

This paper explores the current vulnerable road users (VRU) protection testing procedures, particularly focusing on enhancing bicyclist head protection against car impacts. Existing protocols predominantly involve leg and head impact tests using mechanical impactors, with recent expansions to include assessments of frontal car areas such as bumpers, hoods, headlamps, and windscreen regions [6-9]. However, these requirements are originally based on pedestrian impact conditions, potentially introducing a bias toward pedestrian protection over bicyclist safety. Given the differing initial posture, height, impact speed, and kinematics between pedestrians and bicyclists, there

P. Lozano (pablo.lozano@idiada.com, +34 645 07 40 36) MSc, is a Research Industrial Engineer and A. Gravina (alessandro.gravina@idiada.com) is a Senior Engineer both at Applus IDIADA. Y. Takahashi is the Chairperson of Pedestrian Protection Experts Group at the Japan Automobile Manufacturers Association, Inc.

is a need to assess whether the current testing protocols adequately cover bicyclist injuries and accurately represent the impact conditions experienced by bicyclists.

Some protocols have expanded the headform test area to cover areas normally impacted by bicyclists in case of collision. While this expansion is a step forward in addressing real-world bicyclist scenarios, the impact conditions of these protocols remain the same in these regions, assuming that the head impact conditions of a cyclist are the same as the head impact conditions of a pedestrian. This brings to light a crucial question: are the head impact conditions experienced by cyclists truly analogous to those of pedestrians? While current protocols assume uniformity in impact conditions across different scenarios, the differences between the kinematics involved in cyclist and pedestrian collisions remain insufficiently explored. Consequently, the effectiveness of utilising identical headform impact conditions across these areas remains uncertain. This study aims to address this gap by thoroughly investigating the head impact conditions for cyclists in simulated car-bicycle collisions, thus providing valuable insights to refine and enhance safety testing protocols in the future.

II. METHODS

The study employed a three-phase methodology to investigate bicyclist head impact conditions against a car in car-to-bicycle collisions. In Phase 1 (Load Case Definition), European data from the Initiative for the Global Harmonization of Accident Data (IGLAD) database [10] was analysed, filtering relevant European car-bicycle collision scenarios. This phase involved detailed accidentology analysis, identifying key parameters such as impact speeds or impact angle. Phase 2 focused on Computer-Aided Engineering (CAE) simulations, utilising a human body model (HBM) developed in a previous study [11] and four generic vehicle models: family car, SUV, roadster, and multi-purpose vehicle. A simulation matrix was developed using Optimal Latin Hypercube Sampling (OLHS) techniques, resulting in 32 simulations that covered a broad range of relevant collision scenarios. The final phase, Phase 3, focused on developing a statistical surrogate model to provide a robust assessment of cyclist-car collisions, utilising a Response Surface Model (RSM) to predict and analyse head impact kinematics with optimal computational efficiency. The results from these three phases were used to evaluate the current subsystem test procedures for pedestrian protection [6][7]. This evaluation compared the simulation and surrogate results against existing test procedures, identifying potential gaps in bicyclist protection.

Phase 1: Load Case Definition

An investigation into road accidents involving bicyclists was carried out utilising data from the IGLAD database [10]. The choice of IGLAD as the primary data source for accident statistics was deliberate, given its coverage, particularly within the European Union (EU). As this study aimed to cover the complete European perspective, there was a need to use a database with detailed information from several countries. The only accessible database with those characteristics was the IGLAD. The data used in this research corresponds to IGLAD's Phase III, which provides detailed information from nine countries in the EU (Austria, Czech Republic, France, Germany, Greece, Italy, Spain, and Sweden) and offers data spanning from 2007 to 2018, making a total of 7055 registered cases. A selection criterion was defined to filter only the cases of interest for the bicyclist safety analysis, as shown in Figure 1. The resultant distribution of data after applying the selection criteria is shown in Figure 2.

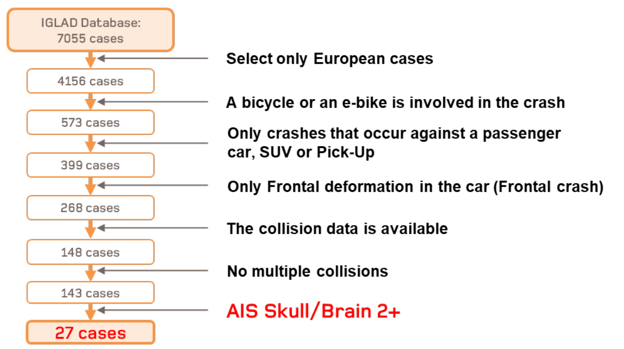

Fig. 1. Selection criteria to filter relevant bicyclist collisions from the IGLAD Database. Only Skull/Brain AIS 2+ injuries were considered in the study.

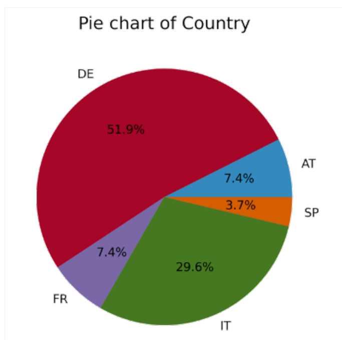

Country	Abbreviation
Germany	DE
Italy	IT
Austria	AT
France	FR
Spain	SP

Fig. 2. Country distribution of the extracted cases from IGLAD after the selection criteria were applied.

Twentyseven cases passed the selection criteria and were used in the analysis. These data points were used to characterise car-to-bicycle collisions with injuries to the skull, brain, and face sustained by bicyclists.
For collision characterisation, the following parameters were considered: bicycle collision speed, car collision speed, impact angle, specific deformation area, and car type (used as a reference).

Collision speeds were defined as the speed of the vehicle (car/bicycle) in km/h at the time of collision. They were the same speed to be used in the simulation phase of the study. They did not take into account any active safety systems that the vehicle may have activated before the collision as this parameter only focused on the final velocity the car reached right before starting the collision.

The impact angle was defined as the angle between the car and the bicycle at the time of impact. As registered in IGLAD, the reference for the angle calculation was the car and the angle was calculated in steps of 30º. If the car and the bicycle were heading in the same direction, the impact angle was 0 degrees. If the bicycle was heading towards the car, the impact angle was defined as 180 degrees. All the ranges in between were defined as positive angles if the bicycle was heading to the right side of a car and negative angles if it was heading toward the left side. Figure 3 illustrates examples of angles to enhance comprehension.

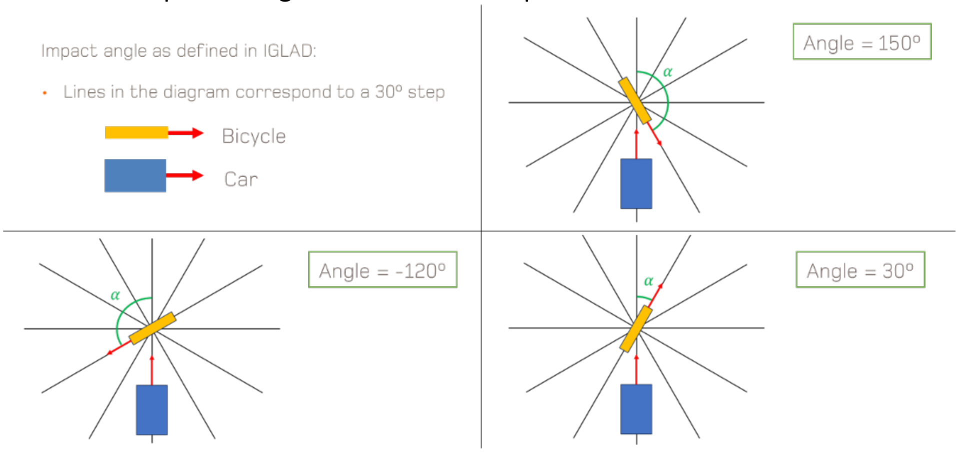

Fig. 3. Impact angle definition according to the IGLAD database. Three examples of impact angles are shown. The car is identified in blue and the bicycle is identified in yellow.

The specific deformation area of the car referred to the precise lateral location of the damage, which corresponded to the impact location in the front of the car. The impact location was classified in the left, middle, or right.

Regarding injury outcomes, the study focused on two key parameters: Skull-Brain Abbreviated Injury Scale (AIS) [12] and Face AIS (used as a reference). These parameters were selected to assess the severity of injuries sustained in the head region in the 27 collisions extracted from the database.
This part of the study was two-fold: first, investigate the range of each parameter to study their variability and significance in the collision scenarios and analyse the influence of each parameter on Skull-Brain AIS, aiming to identify the main factors contributing to head injuries in car-bicycle collisions. Second, an association analysis was conducted to investigate the relative influence of the selected parameters. For continuous variables, linear correlation was assessed using the Pearson correlation coefficient. However, for discrete variables, Theil's U (Uncertainty coefficient) [13] was utilised as it provided a better representation of asymmetric associations. Additionally, the association between continuous and discrete variables was evaluated using the Correlation Ratio [14]. This analysis was performed using Python 3.10.6 [15] and the library dython [16].

Lastly, a simulation matrix was calculated for the CAE simulation study. A Design of Experiments (DoE) was carried out by applying Optimal Latin Hypercube Sampling (OLHS) [17]. The objective was to cover at least 70% of the population data observed from IGLAD to capture a significant part of the European population. The simulation matrix was calculated in three steps:

1. First, the most relevant parameters from the accidentology study were identified based on the association analysis.
2. Secondly, the ranges of those parameters were set to reach the goal of population coverage. From the 27 points extracted from IGLAD, at least 70% of those points should be inside the ranges set for the

parameters, meaning that at least 19 out of the 27 points should meet the conditions proposed in the simulation matrix.

3. Extra variables not represented in IGLAD were added for an adequate definition of each simulation. These include the pedalling posture of the HBM and the type of car to be used. Four postures and four car models were selected to properly cover different possibilities that may occur on the road.

Phase 2: CAE Simulation Study

The focus of Phase 2 was to study via simulation how some input variables (defined in Phase 1) affected the bicyclist's head kinematics and impact conditions against the car in the case of car-to-bicycle collision. To achieve this objective, car-bicycle impact simulations were run using the simulation matrix proposed in Phase 1. Based on the results from the simulation study, a series of response surfaces were generated to predict head impact location, head impact angle, and head impact velocity in Phase 3 of the study.

The simulation model consisted of a car model, a bicycle model, and a VRU HBM. Based on the simulation matrix, a certain initial velocity was given to the car model in its longitudinal direction. The car models used for this study were versions of the European New Car Assessment Programme (Euro NCAP) TB024 [18] car models. These models are currently used for the certification of pedestrian HBMs and are modelled to reproduce a similar hood deformation to that of a generic full-car model. For this purpose of HBM certification, four generic vehicle models exist and were used in this study: a family car (FCR), a sport utility vehicle (SUV), a roadster (RDS), and a Multi-Purpose Vehicle (MPV) model. These models were adapted to the requirements of this study. To meet the different simulation conditions, lateral surfaces were added to the sides of the car models to better represent the geometry of a real car and to have realistic HBM kinematics in the simulations. The side surfaces were generated starting from the surfaces already present in each model and considering average width obtained from a benchmarking analysis.

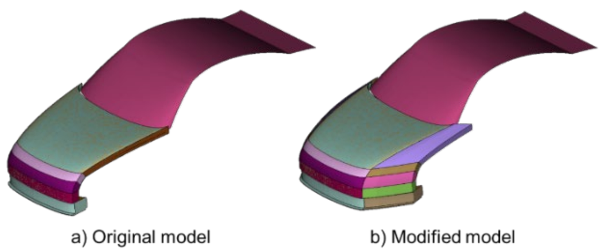

Fig. 4. RDS simulation model. On the left (a) is the original model from TB024, and on the right (b) is the modified model with the lateral surfaces to complete the geometry of the car frontal structure.

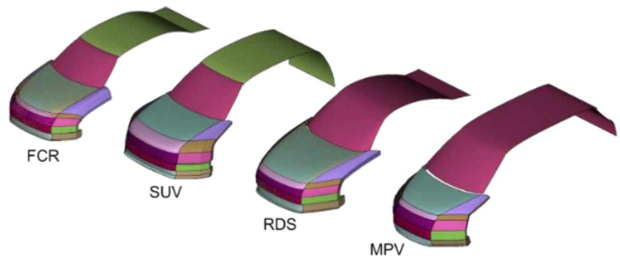

Fig. 5. The four modified TB024 car models used in the study. From left to right: FCR, SUV, RDS, and MPV models.

The bicycle model represented the majority of the Japanese bicycle fleet. Both the structure and the wheels of the bicycle were validated against [19]. The bicycle and HBM were transformed based on the simulation matrix to match the impact angle, and an initial translational velocity was applied to both models. The wheels of the bicycle had the corresponding rotational velocity.

The HBM used in this study was taken from a previous study [11]. This HBM was developed with a special focus on pedestrian safety and can be divided into two sections: the upper and the lower sections of the body. The upper body section, composed of the head, neck, torso, and upper/lower arms, is a kinetic chain composed of rigid body segments that recreate realistic kinematics of a human body. The lower section composed of the lumbar section of the spine modelled as articulated rigid bodies and more detailed finite element pelvis and lower limb models. This HBM can represent different patterns of injuries in the lower limbs and was validated against 40km/h car impacts in a pedestrian posture [20]. Images from the simulation model setup can be found in Appendix B.

Phase 3: Analysis of Results and Statistical Surrogate Model Development

Surrogate models are in general, part of a *black modelling* approach as they are not based on physics but can predict output variables based on defined input values. The benefit of this approach is significant CPU time savings compared to a Finite Element (FE) simulation. Due to the time constraints of the project, a limited number of FE simulations were run. Nevertheless, the possible combinations of parameters in car-to-bicycle collisions in Europe can be extensive. Therefore, a surrogate model was calculated based on the results of the FE simulations to increase the coverage of the study. The main goal was to be able to predict each of the simulation outputs such as head impact location, head impact angles, or head impact velocity, from simulation inputs such as bicycle and car collision speeds or impact angle. A Response Surface Model (RSM) was selected as a surrogate model. The RSMs developed in this study used second-order polynomials due to the limited number of simulation data points. The general formula of the RSMs used is the following:

$$F(x) = a_0 + \sum b_i x_i + \sum c_{ii} x_i^2 + \sum c_{ij} x_i x_j \; (i < j) \qquad (1)$$

Where a_0 is the constant, b_i are the linear coefficients, c_{ii} are the quadratic coefficients, and c_{ij} are the interaction coefficients. x_i and x_j represent the different input variables of the RSM.

Based on the simulation results, several response surface models were developed, one for each of the outputs extracted from the simulation. This was performed in five steps. The highest influencing input-output parameters were identified using a Spearman's correlation map. Secondly, a detailed analysis of the results was performed by analysing 2D scatter plots only for the interactions between input and output parameters with higher correlation (based on the correlation map generated in the first step). Thirdly, the RSMs were calibrated with polynomial coefficients for each output. Afterwards, an error evaluation of each RSM was performed using the normalised root mean square error (RMS), the coefficient of determination (R^2), and the adjusted R^2. Lastly, five extra simulations with randomised input variables were used to perform a verification of the response surface models.

III. RESULTS

Phase 1: Load Case Definition

The accidentology analysis focused on identifying the following four parameters: bicycle and car collision speeds, impact angle, and the specific deformation area or impact point referenced to the car. The range and distribution of each parameter are shown in the following Figure.

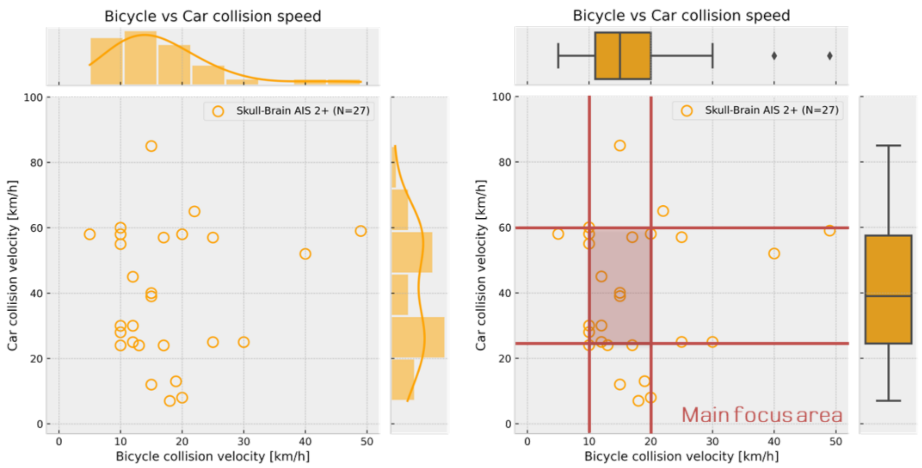

Fig. 6. Bicycle vs car collision speed. On the left side, the distribution of the input parameters can be observed. On the right, box plots depict the prevalent conditions associated with bicycle-car collisions.

Bicycle collision speeds were mostly lower than 30 km/h, while car collision speeds ranged mostly between 10 and 60 km/h. 25th and 75th percentiles were calculated as well to depict the most prevalent conditions associated with bicycle-car collisions.

Regarding the impact angle, Figure 7 shows the distribution of the impact angle among the 27 different cases and the associated Skull/Brain AIS level for each data point. It can be observed that most of the collisions happened over 90 degrees and under –90 degrees, with most collisions occurring at –120 degrees. Also, 0 degrees or frontal collisions were observed within the data. Regarding injury criteria, no big differences were observed between the different impact angles. Most of the impact angles present a certain number of AIS 2 cases and a few AIS 3+ cases, indicating that no impact angle is more likely than the rest to have a specific level of injury. However, this concept will be further analysed in the association matrix section. Regarding the specific car deformation area, 48.15% of the deformations in the front area of the car were concentrated on its left side. Another important set of collisions occurred on the right side of the front of the car (37%), showing that the least likely impact point of the bicycle tends to be the middle of the car. This also suggests that most collisions may occur when turning rather than in normal driving situations. Interestingly, the collisions resulting in the highest severity values for Brain/Skull AIS level predominantly occurred when the impact location was on the right side of the car. This observation underscores the asymmetrical distribution of impact severity across different regions of the vehicle, shedding light on potential patterns in injury outcomes related to collision kinematics.

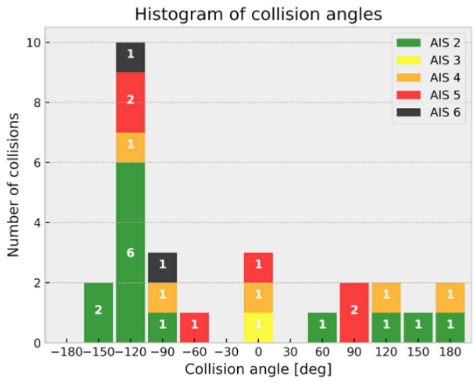

Fig. 7. Histogram of collision impact angles and their respective Brain/Skull AIS level.

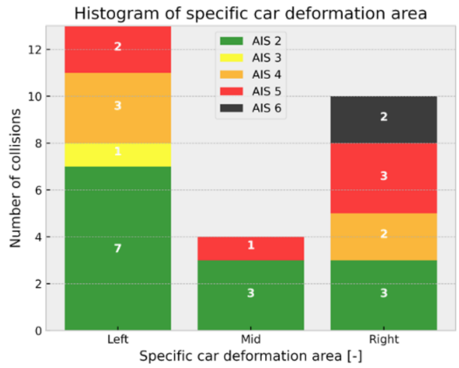

Fig. 8. Histogram of specific car deformation areas and their respective Brain/Skull AIS level

Lastly, an association analysis between collision definition data and injury outcome of each of the 27 data points was performed. The objective was to investigate the correlation value between each of the variables previously studied and the head injury that the bicyclists suffered. The association matrix is shown in Figure 9.

Scale of correlation coefficient	Value
$0 < r \leq 0.19$	Very Low Correlation
$0.2 \leq r \leq 0.39$	Low Correlation
$0.4 \leq r \leq 0.59$	Moderate Correlation
$0.6 \leq r \leq 0.79$	High Correlation
$0.8 \leq r \leq 1.0$	Very High Correlation

Fig. 9. Association matrix between input parameters and injury outcomes (left) and scales of association coefficients (right).

The association matrix revealed notable correlations between car collision speeds and Skull-Brain AIS, with a coefficient of 0.67, indicating a strong relationship. Additionally, impact angle and bicycle collision speed exhibited moderate correlations with Skull-Brain AIS, at coefficients of 0.43 and 0.40, respectively. These results showed how highly the brain injury that the cyclist may suffer is correlated with the collision speed of the car and the bicycle, increasing the likelihood of injury with the speed increase. The type of car and the impact point, however, did not show significant relevance regarding brain injury.

Based on the association matrix and the overall accidentology study, a simulation matrix was designed for the simulation phase. Car collision speed, bicycle collision speed, impact angle, and specific deformation area were chosen based on the correlation values with injury outcome and the observed distribution. Once these parameters were identified, the variable ranges were calculated in an iterative way to reach the coverage goal of at least 70% of the EU population. The variables and ranges included in the simulation matrix are shown in Table

I.

TABLE I
VARIABLES AND RANGES USED TO DEFINE THE SIMULATION MATRIX

ID	VARIABLE	VALUES/RANGES
1	Pedaling posture	PP1, PP2, PP3, PP4
2	Type of car	FCR, MPV, RDS, SUV
3	Car collision speed	From 5 to 60 km/h [steps of 5km/h]
4	Bicycle collision speed	From 5 to 30 km/h [steps of 5km/h]
5	Specific car deformation area	Left, Mid, Right
6	Impact angle	± 0, 90, 120,150,180

The proposed ranges for the matrix eventually covered 77.8% of the IGLAD cases, successfully reaching the goal of coverage. Applying the OLHS methodology, a 32-simulation matrix was generated based on the defined variables and ranges. The resultant matrix can be found in Appendix A.

Phase 2: CAE Simulation Study

The 32 simulations were run using a right-handed Cartesian coordinate system oriented relative to the vehicle model. The X-axis extends longitudinally along the length of the vehicle, with positive values increasing from the front toward the rear of the car. The Y-axis represents the lateral direction, extending across the width of the vehicle, and the Z-axis represents the vertical direction, with Z=0 at ground level and positive values increasing with height. The following variables were obtained for each load case: time of head impact, X, Y, and Z coordinates of head impact location, X, Y, and Z components of head impact velocity, head impact velocity magnitude, head impact angles, and Brain Injury Criteria (BrIC). Figures 10 and 11 show the head trajectory and final impact of one of the simulations, as well as the coordinate system used.

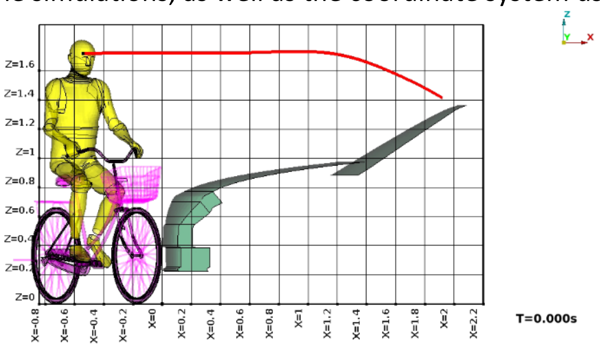

Fig. 10. Lateral view of the simulation setup. The head trajectory is shown in red.

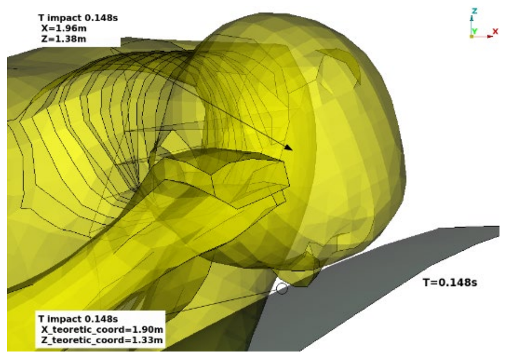

Fig. 11. HBM head at the time of impact. Both the Center of Gravity (CoG) and contact point of the head coordinates are shown.

Phase 3: Statistical Surrogate Model Development

A correlation map was obtained for all the inputs and outputs as shown in Figure 12. There were many moderate correlations and 2 high-correlation cases. Car collision speed showed a high correlation with the head X coordinate and with the head magnitude of velocity.

	X_coor (m)	Y_coor (m)	Z_coor (m)	Mag_vel (km/h)	Alpha (deg)	Beta (deg)	Gamma (deg)	BrIC	X_vel (km/h)	Y_vel (km/h)	Z_vel (km/h)	wx (rad/s)	wy (rad/s)	wz (rad/s)	T_imp (s)
Bicycle collision speed	0.43	0.32	0.11	0.36	0.36	0.10	0.33	0.22	0.34	0.39	-0.22	0.36	0.18	0.16	-0.52
Car collision speed	0.66	-0.02	0.34	0.68	-0.05	0.36	-0.06	0.44	0.57	0.10	-0.47	0.23	0.56	0.08	-0.70
Impact angle	-0.09	-0.12	0.14	-0.03	0.09	0.28	-0.15	0.25	0.08	0.03	0.11	-0.19	0.21	0.29	0.03
Impact location from car	0.17	0.51	0.10	0.06	-0.06	0.03	-0.04	-0.25	0.15	0.01	-0.09	-0.06	-0.27	-0.06	0.09
Pedaling Posture	-0.08	0.07	0.20	0.04	-0.10	0.14	-0.18	-0.14	0.13	-0.16	-0.02	-0.26	-0.12	-0.07	-0.08
Type of car	0.25	-0.09	0.09	0.23	-0.36	0.02	-0.26	-0.30	0.31	-0.30	-0.21	-0.31	-0.30	-0.45	0.00

Fig. 12. Correlation map between input and output variables. The correlation map indicated in red direct correlation (1) and blue indicated an inverse correlation (-1). The colours in between are adjusted based on the correlation coefficient.

As shown in Figure 15, among the six independent variables analysed in this DOE study, three have demonstrated moderate to high correlation with the output variables under investigation, while the remaining variables show only low correlation. The three variables with the strongest correlation, ranked in the order of significance, are car collision speed, specific deformation area/impact location, and bicycle collision speed. Notably, the location of impact from the car predominantly affects the Y coordinate of the head impact. To facilitate further global optimisations of the system, a surrogate model of the response surface type was calibrated, and its error was scrutinised. An example of the polynomial coefficients for the X coordinate of the head can be found in Figure 13.

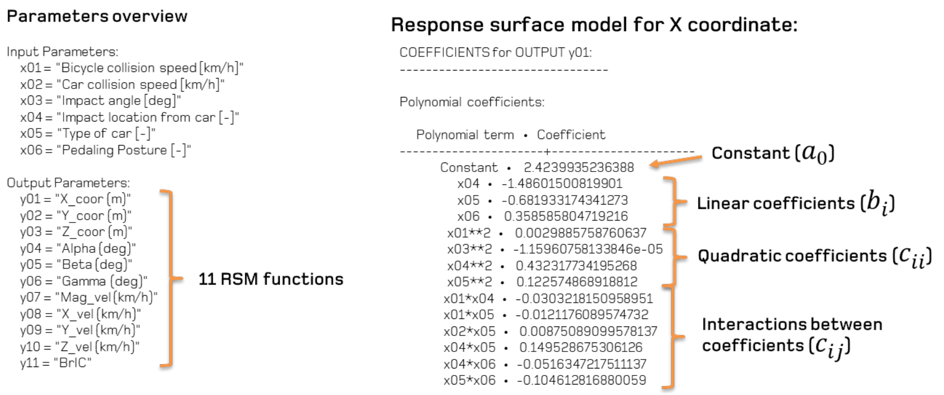

Fig. 13. Example of RSM to predict X coordinate of the head based on the input parameters. On the left, the input and output parameters are indicated. On the right, the response surface model coefficients for the X coordinate are presented, indicating each type of coefficient.

Each RSM is unique for each output parameter,each one having different polynomial coefficients. Lastly, an error analysis was performed to measure the accuracy of the approximation that was performed when generating a RSM. The results showed that four RSMs have proven perfect relationships to those of the responses of the physical model from which they were derived (gamma, magnitude of velocity, X velocity, and Y velocity). Three showed a very strong relationship, two showed a strong relationship, and two showed a moderate relationship. The RSMs can be found in Appendix C.

Responses	Normalized RMS error	R^2	Adjusted R^2	Relat.
X coordinate [m]	0.125	0.79	0.74	VS
Y coordinate [m]	0.163	0.58	0.46	S
Z coordinate [m]	0.164	0.67	0.58	VS
Alpha [deg]	0.127	0.49	0.35	M
Beta [deg]	0.173	0.43	0.28	M
Gamma [deg]	0.085	0.82	0.77	P
Magnitude velocity [km/h]	0.093	0.87	0.84	P
X velocity [km/h]	0.123	0.86	0.82	P
Y velocity [km/h]	0.097	0.82	0.77	P
Z velocity [km/h]	0.131	0.63	0.54	S
BrIC	0.105	0.80	0.75	VS

Fig. 14. Error analysis of each RSM. The column on the right indicates the level of relationship: P=Perfect, VS=Very Strong, S=Strong, and M= Moderate.

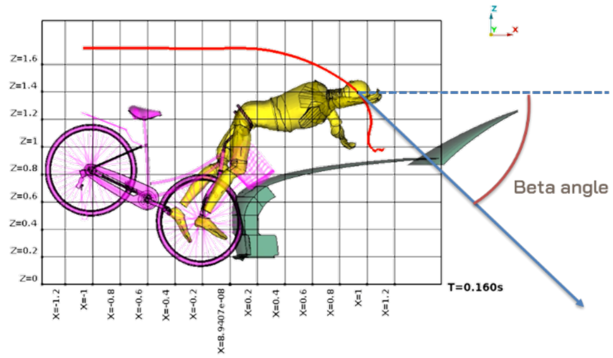

Fig. 15. Beta angle of the head calculated from the X velocity of the head (Vx) and the Z velocity of the head (Vz).

The beta angle (described in Figure 15) is the rotation of the head around the Y-axis and it was calculated using the Vx and the Vz of the head at the time of collision. Similarly, the gamma angle is the rotation of the head around the Z-axis and was calculated using Vx and Vy.

Gap Identification with Current Testing Procedures

The RSMs were used to calculate the head impact location, magnitude of head impact velocity, and beta angle of all the possible combinations derived from the list of variables determined by the accidentology study shown in Table II. These three variables determine the headform test conditions that are currently being used. A total of 31680 cases were computed from a full-factorial combination of the variables and ranges shared in Table I.

For the analysis of the head impact location, both results from full HBM simulations and RSMs were analysed. The simulation results are presented in Figure 16. The head impact locations were very dispersed, but some tendencies were observed when comparing the four cars. In 26% of the simulations, the head contact occurred near the cowl area. Also, some simulations landed near other parts of the car, such as the A-pillars or the windscreen-hood connection. RSM results are presented in Figure 17. The obtained RSM points showed that the upper part of the hood, the full windscreen, and the start of the roof were highly dense regions of head impact collision points, further supporting the tendency observed in the simulations.

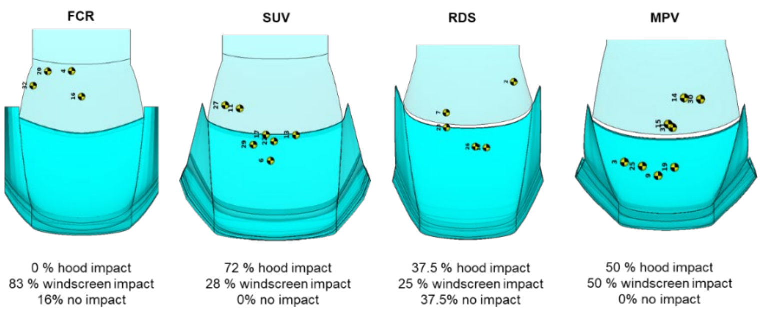

Fig. 16. Comparison of head impact location in the four car models. Twentysix percent of the simulations landed in the cowl area, a high-rigidity area that may pose an increased risk of injury. Five simulations also landed near other regions like the A-pillar or the windscreen-hood connection.

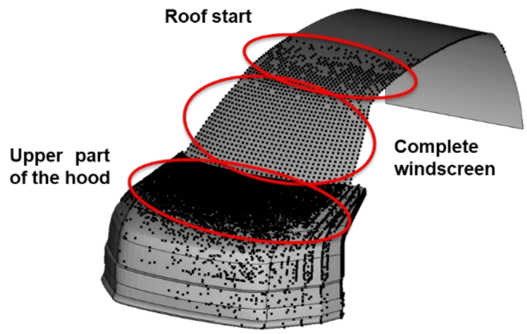

Fig. 17. RSM head collision coordinates plotted over the SUV car model. The hood, windscreen and roof start were highly dense regions.

Both the simulations and RSMs were analysed regarding the magnitude of the velocity of the head impact. The magnitude of velocity was calculated using the three components of the velocity and calculating the magnitude for both the simulation and the RSM. Histograms were calculated for both the simulated cases and the statistical model cases.

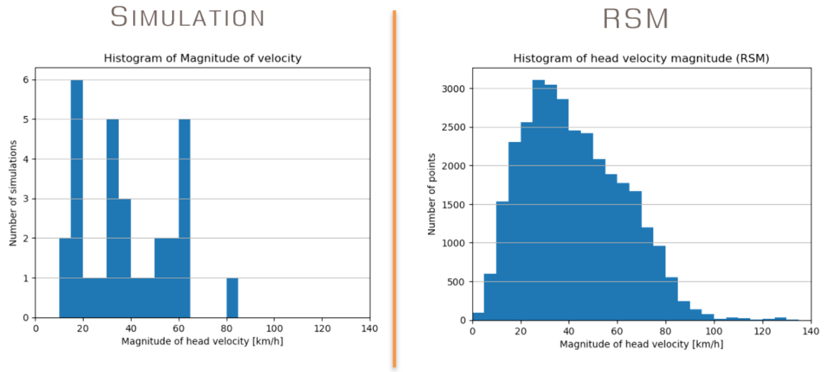

ALL CASES

Statistics [km/h]	
Mean	42.23
SD	20.40
Min	1.4
25%	26.31
50%	39.52
75%	56.81
Max	138.68

Fig. 18. Histograms of the magnitude of velocity. On the left is the simulation histogram, and on the right is the RSM histogram with all the cases (hood and windscreen cases) and the main statistics.

Simulations showed three peaks of head impact velocity at 20, 35, and 60 km/h. The RSM showed that the most common impact velocity was around 40 km/h. The mean and the median of the calculated points were also around 40 km/h. Also, 58% of the cases had an impact velocity higher than 35 km/h. It should be noted, however, that these results assume a uniform distribution of load cases within the ranges of the collision parameters assumed for this study. Moreover, the windscreen cases were isolated to study the impact conditions of those specific points. The windscreen impact area was included in the regulation to cover bicyclists. However, the same impact conditions of the adult pedestrian were maintained. The statistics presented in Figure 19 show that the velocity in this area might be even higher, assuming the bicycle type of a Japanese city cycle.

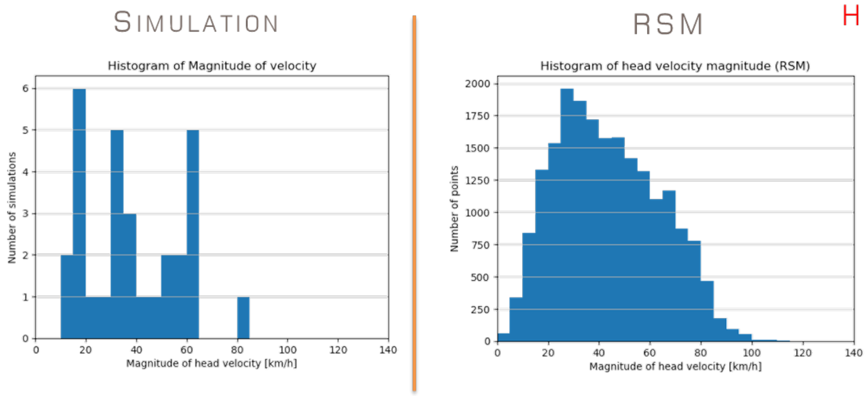

HEAD TO WINDSCREEN CASES

Statistics [km/h]	
Mean	43.61
SD	20.22
Min	1.4
25%	27.4
50%	41.62
75%	58.72
Max	111.93

Fig. 19. Histograms of the magnitude of the velocity of the head. On the left is the simulation histogram, and on the right is the RSM histogram with only head-to-windscreen cases and the main statistics.

A similar procedure was followed regarding the headform impact angle. The head impact angle was calculated from the head Vx and Vz and was defined in this study as the beta angle. The beta angle had negative values in most of the simulations as most of the head impact collisions had negative Vz, indicating a velocity towards the ground (in the direction of gravity). With this system, the impact angle for the adult headform used by the current subsystem test procedure is -65 degrees, indicating 65 degrees from the horizontal, as indicated in Figure 15. Simulations showed three angles as the most frequent ones: -80, -55, and -40 degrees. The full-factorial model showed that most of the cases landed between -65 degrees (the current regulation configuration) and -50 degrees, showing a more horizontal impact angle for the head of a bicyclist compared to the impact condition of a pedestrian. This is shown in Figure 20.

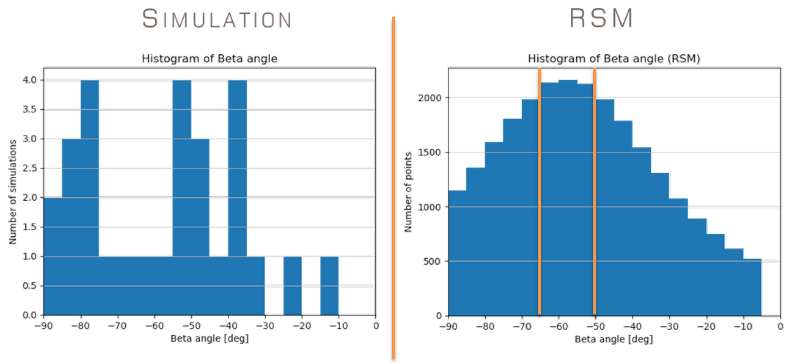

ALL CASES

Statistics [deg]	
Mean	-59.03
SD	34.51
Min	-194.52
25%	-79.02
50%	-58.42
75%	-38.33
Max	72.99

Fig. 20. Histograms of Beta angle. On the left is the simulation histogram, and on the right is the RSM histogram with all the cases (hood and windscreen cases) and the main statistics.

When isolating windscreen cases (Figure 21), an increase in the beta angle is observed, and a clear tendency appears regarding windscreen head impact collisions. The statistics show that the mean value and the most frequent windscreen case land on an angle of -50 degrees.

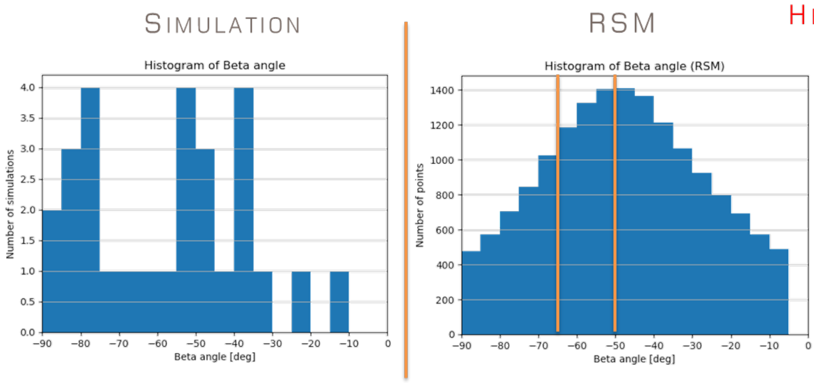

HEAD TO WINDSCREEN CASES

Statistics [deg]	
Mean	-50.7
SD	35.28
Min	-187.99
25%	-69.96
50%	-49.55
75%	-29.37
Max	72.99

Fig. 21. Histograms of beta angle. On the left is the simulation histogram, and on the right is the RSM histogram with only the windscreen cases and the main statistics.

IV. DISCUSSION

The current subsystem test procedure for pedestrian protection aims to reduce the severity of injuries to pedestrians (and bicyclists, as amended by the 03 series of UN R127) struck laterally by vehicles in collisions at 40 km/h and below. The test procedure was designed to simulate pedestrian impacts at various locations on the vehicle, including the bonnet (hood), windscreen, bumpers, and other relevant components, to evaluate their safety performance against a pedestrian body.

This study focused on head impact conditions of bicyclists in collisions with vehicles. The EEVC subsystem test procedure uses the headform to represent head impact against the surface of a car in the vertical longitudinal plane, focusing on lateral impact to a pedestrian from a car. The headform test procedure is conducted in a controlled environment, typically within a laboratory or testing facility. The vehicle under evaluation is positioned according to specified parameters, such as distance and angle, relative to the test equipment. A headform impactor is used to measure the accelerations that a pedestrian's head may suffer in case of collision. There are adult and child headform impactors, and each one is used in a specific testing location. These headforms are then positioned at predetermined locations and orientations relative to the vehicle's front-end structure and propelled toward the vehicle at a specific velocity and angle, simulating head impact in a pedestrian collision. Based on this information, the three most relevant variables that define the current test procedure are the impact location, the magnitude of the impact velocity, and the impact angle of the headform.

In the first place, the impact test area is mainly defined by the Wrap Around Distance (WAD) which is the geometric trace described on the outer surface of the vehicle front structure by one end of a flexible tape when it is held in a vertical longitudinal plane of the vehicle and traversed across the front structure [7]. Recently, an amendment was added to this test procedure, increasing the testing area potentially up to the windscreen. The rear end of the current test area goes from WAD 1700 up to WAD 2500 or a line 130 mm forward to the rear visible edge of the windscreen material. The RSM generated in this study showed that 20266 points (64% of the cases) landed in the windscreen area, indicating that increasing the testing area up to the WAD 2500 may be a positive decision towards bicyclist safety.

Regarding the magnitude of velocity, it is highly related to the acceleration measured in the headform at the time of impact and, therefore, related as well to the HIC values calculated from the head acceleration. The statistics presented in this study showed that the head impact velocity in the windscreen area could be higher than 35 km/h.

Lastly, the impact angle refers to the orientation of the headform impactor during testing. As per the current test procedure, this angle is set at 50 and 65 degrees for the child and adult headform, respectively, as defined downward from the horizontal line. The RSMs generated in this study showed an increase in beta angle when isolating the head-to-windscreen cases. A tendency appeared regarding windscreen head impact collisions. Results showed that the mean value and the most frequent windscreen case landed on an angle of -50 degrees, indicating that the impact angle of a bicyclist may be on average smaller than that of a pedestrian. The use of a smaller impact angle to represent bicyclist impact could be a potential measure to enhance protection against a bicyclist, depending on the relevance of the assumptions set by this study.

It should be noted that the RSM results discussed in the previous paragraphs were obtained using the range of load cases described in Table I, which is not necessarily consistent with the assumptions behind the test procedure. For example, the car speeds above 40 km/h that are not within the scope of the current test procedure were included in the load cases investigated in this study. In addition, the analyses of the RSM results assumed uniform distribution of the load cases within the range, which means that the results are not compensated for the distribution of the load cases in real-world accidents. Further analyses are necessary to compare predicted head impact conditions directly with the test conditions currently used.

V. LIMITATIONS

The following aspects may have affected some of the results obtained in this study:

- A limitation arises from the filtering process during Phase 1 of accidentology analysis, where only 27 cases met the necessary criteria for inclusion. This results in a small sample size for the comprehensive European study region, posing constraints on the generalisability of findings.
- There was a disproportionate representation of data in the 27 selected cases from Phase 1. Figure 2 shows that 51.9% of the cases were located in Germany, 29.6% in Italy, 7.4% in Austria, 7.4% in France, and 3.7% in Spain. The findings from this first phase could be biased due to uneven data representation.
- The distribution of load cases within the range of collision parameters specifically determined for this study was assumed to be uniform. The distribution of the output parameters, therefore, would be biased, although the range of the output parameters would correspond to the range of the collision parameters used in the study.
- Only one HBM and one bicycle model were used for this study. The conclusions drafted may not cover the complete population of bicyclists in Europe.
- Four simplified car models were used with rigid windscreens. Therefore, HIC injury metrics were not calculated, and the deformation of the windscreen was not taken into account for this study. Detailed body-to-car interactions might not be captured in the study.

The study hereby presented aimed to cover a large part of the EU population of bicyclists in defining the load cases, while the CAE simulations used a bicycle model representing the most popular type of bicycle in Japan. This may have posed some discrepancy between the results of the study and field observations either in Europe or in Japan, which also needs to be further clarified in a future study.

VI. CONCLUSION

The study has presented the methods and results employed for conducting statistical analysis of bicyclist accidents in the EU and investigating bicyclist safety via HBM simulations. These procedures were applied to gather significant outcomes, potentially providing insight into future modifications of the current test procedure for VRU protection.

The research demonstrated that statistical analysis could effectively define ranges for car collision speed, bicycle collision speed, impact angle, and specific car deformation area to cover 77.8% of the bicyclist collision population in Europe. Kinematics of bicycle-car collisions were simulated using HBMs based on these variables and ranges. Moreover, eleven RSMs were developed to predict with computational efficiency the head kinematics of a bicyclist from collision characterisation variables such as car impact speed, bicycle collision speed, or impact angle. These RSMs were shared in the study. Results can be used to gain insight into potential future modifications to current test procedures to better protect VRUs, including bicyclists.

Lastly, the study successfully developed useful technical information, data, and tools that can be used to investigate effective and realistic measures for modified test procedures to further enhance VRU head protection, specifically focusing on the head protection of a bicyclist as well as head impact against the front windscreen.

VII. ACKNOWLEDGEMENTS

This work was carried out at Applus IDIADA, Tarragona, Spain, and funded by the Japan Automobile Manufacturers Association, Inc. (JAMA), Tokyo, Japan. The authors would like to thank JAMA for the collaboration opportunity.

VIII. REFERENCES

[1] EU Urban Mobility Observatory, "Best practice in boosting cycling modal share and creating safe, sustainable cities - European Commission." Accessed: Feb. 17, 2025. [Online]. Available: https://urban-mobility-observatory.transport.ec.europa.eu/resources/case-studies/best-practice-boosting-cycling-modal-share-and-creating-safe-sustainable-cities_en

[2] United Nations, "Promoting Cycle Day initiatives as a way to adopt non-motorized transport policies in the city to make cities inclusive, safe and sustainable | Department of Economic and Social Affairs." Accessed:

Feb. 17, 2025. [Online]. Available: https://sdgs.un.org/partnerships/promoting-cycle-day-initiatives-way-adopt-non-motorized-transport-policies-city-make#description

[3] A. Gaur, S. Gupta, and R. K. Upadhyay, "Integration of Cycling with Public Transportation," in *Intelligent Transportation System and Advanced Technology*, R. K. Upadhyay, S. K. Sharma, and V. Kumar, Eds., Singapore: Springer Nature, 2024, pp. 177–215. doi: 10.1007/978-981-97-0515-3_9.

[4] L. Rothman *et al.*, "330 Pedaling forward: the evolution of bicycling infrastructure in 3 Canadian cities from 2010 to 2022," *Inj Prev*, vol. 30, no. Suppl 1, p. A72, Sep. 2024, doi: 10.1136/injuryprev-2024-SAFETY.169.

[5] European Commission, "Collision Matrix: Road Traffic Fatalities in the EU in 2021." 2023.

[6] United Nations, "GTR no. 9, Pedestrian safety: proposal to develop amendments to Global Technical Regulation no. 9, Pedestrian safety. / submitted by the representative of Japan." United Nations. Economic and Social Council, Aug. 28, 2009. Accessed: Feb. 19, 2025. [Online]. Available: https://digitallibrary.un.org/record/665298

[7] UN/ECE, "UN Regulation No 127 – Uniform provisions concerning the approval of motor vehicles with regard to their pedestrian safety performance [2020/638]." 2016. Accessed: Feb. 19, 2025. [Online]. Available: https://eur-lex.europa.eu/eli/reg/2020/638/oj

[8] *Assessment Protocol - VRU v11.4*, Jan. 2023.

[9] *JNCAP Assessment Protocol - Pedestrian Protection*, 2021.

[10] IGLAD consortium, "IGLAD - Initiative for the Global Harmonization of Accident Data." Accessed: Feb. 20, 2025. [Online]. Available: https://www.iglad.org/index.html

[11] Y. Kikuchi, Y. Takahashi, and F. Mori, "Development of a Finite Element Model for a Pedestrian Pelvis and Lower Limb," SAE International, Warrendale, PA, SAE Technical Paper 2006-01–0683, Apr. 2006. doi: 10.4271/2006-01-0683.

[12] "About AIS," Association for the Advancement of Automotive Medicine. Accessed: Feb. 20, 2025. [Online]. Available: https://www.aaam.org/abbreviated-injury-scale-ais/about-ais/

[13] H. Theil, "On the Estimation of Relationships Involving Qualitative Variables," *American Journal of Sociology*, vol. 76, no. 1, pp. 103–154, 1970.

[14] K. Mather, "R. A. Fisher's Statistical Methods for Research Workers: An Appreciation," *Journal of the American Statistical Association*, vol. 46, no. 253, pp. 51–54, 1951, doi: 10.2307/2280093.

[15] "3.10.6 Documentation," Python 3.10.6 documentation. Accessed: Jan. 30, 2025. [Online]. Available: https://docs.python.org/release/3.10.6/

[16] S. Zychlinski, *dython*. (2018). Python. Accessed: Jan. 30, 2025. [Online]. Available: http://shakedzy.xyz/dython/

[17] J.-S. Park, "Optimal Latin-hypercube designs for computer experiments," *Journal of Statistical Planning and Inference*, vol. 39, no. 1, pp. 95–111, Apr. 1994, doi: 10.1016/0378-3758(94)90115-5.

[18] Euro NCAP, "Technical Bulletin 024. Pedestrian Human Model Certification v4.0." Jul. 2023. [Online]. Available: https://cdn.euroncap.com/media/77683/tb-024-pedestrian-human-model-certification-v40.pdf

[19] R. Nakahara *et al.*, "Influence of Bicycle Deformation and Type on Head Injury Values of a Cyclist in a Car-to-Bicycle Collision," *International Journal of Automotive Engineering*, vol. 10, no. 4, pp. 316–323, 2019, doi: 10.20485/jsaeijae.10.4_316.

[20] Y. Kikuchi, Y. Takahashi, and F. Mori, "Full-Scale Validation of a Human FE Model for the Pelvis and Lower Limb of a Pedestrian," SAE International, Warrendale, PA, SAE Technical Paper 2008-01–1243, Apr. 2008. doi: 10.4271/2008-01-1243.

IX. APPENDIX A – SIMULATION MATRIX

Id	Pedaling Posture	Model	Type of car	Car collision speed	Bicycle collision speed	Impact location from car	Impact angle
1	PP2	A	SUV	45	10	Left	150
2	PP3	B	RDS	30	5	Right	120
3	PP2	A	MPV	10	20	Left	180
4	PP3	B	FCR	45	30	Right	120
5	PP2	A	RDS	60	30	Mid	90
6	PP2	A	SUV	25	25	Mid	150
7	PP2	B	RDS	35	15	Right	0
8	PP3	B	FCR	55	15	Mid	90
9	PP3	B	MPV	10	10	Right	150
10	PP3	B	RDS	35	10	Left	180
11	PP3	B	SUV	50	20	Right	150
12	PP2	A	FCR	45	20	Left	90
13	PP3	B	SUV	20	15	Mid	120
14	PP2	A	MPV	30	5	Left	90
15	PP3	B	MPV	25	5	Mid	0
16	PP2	A	FCR	20	20	Right	120
17	PP1	A	SUV	45	10	Left	-150
18	PP4	B	RDS	30	5	Right	-120
19	PP1	A	MPV	10	20	Right	-180
20	PP4	B	FCR	45	30	Right	-120
21	PP1	A	RDS	60	30	Mid	-90
22	PP1	A	SUV	25	25	Mid	-150
23	PP1	A	RDS	35	15	Right	0
24	PP4	B	FCR	55	15	Mid	-90
25	PP4	B	MPV	10	10	Right	-150
26	PP4	A	RDS	35	10	Left	-180
27	PP4	B	SUV	50	20	Right	-150
28	PP1	A	FCR	45	20	Left	-90
29	PP4	B	SUV	20	15	Mid	-120
30	PP1	A	MPV	30	5	Left	-90
31	PP4	B	MPV	25	5	Mid	0
32	PP1	A	FCR	20	20	Right	-120

Fig. A1. Simulation matrix used in the CAE simulation study.

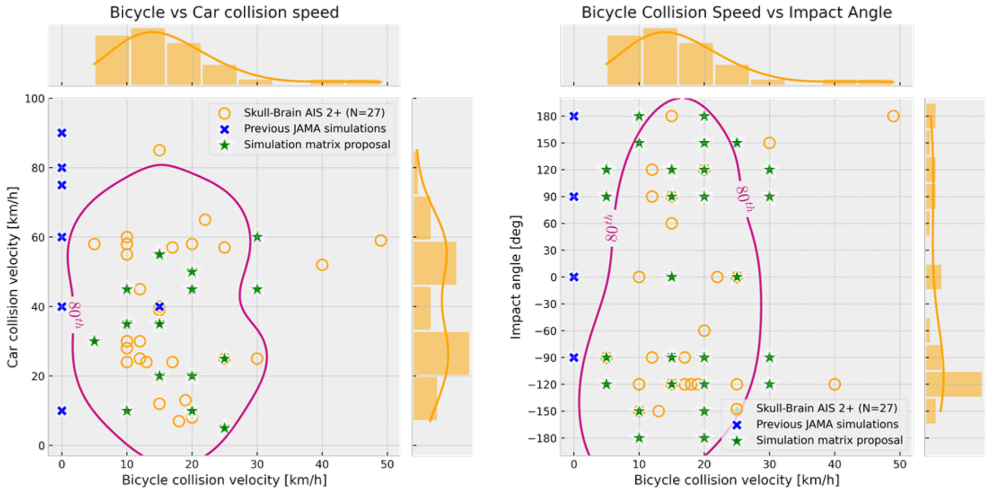

Fig. A2. Simulation matrix visualised over the 27 data points extracted from the IGLAD database. The line shows the region of the 80th percentile of the data, showing the region where 80% of the population data lands.

X. APPENDIX B – SIMULATION MODEL SETUP

The simulation model setup used in this study is shown in the Figures B1 and B2.

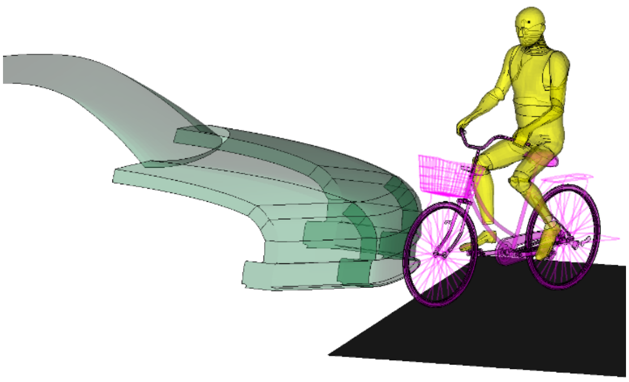

Fig. B1. Isometric view of the simulation model setup. The car is shown in green, the bicycle model in purple, and the HBM in yellow.

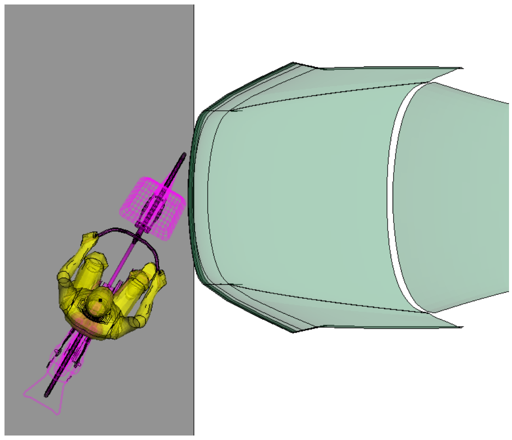

Fig. B2. Top view of the simulation setup.

XI. APPENDIX C – RESPONSE SURFACE MODELS AND ERROR ANALYSIS

Only relations highlighted in orange in Figure C1 with coefficients higher than 0.3 are displayed in 2D scatter plots. Five simulations had no head impact.

	Output parameters no. 1 priority											no. 2 priority			
	X_coor (m)	Y_coor (m)	Z_coor (m)	Mag_vel (km/h)	Alpha (deg)	Beta (deg)	Gamma (deg)	BrIC	X_vel (km/h)	Y_vel (km/h)	Z_vel (km/h)	wx (rad/s)	wy (rad/s)	wz (rad/s)	T_imp (s)
Bicycle collision speed	0.43	0.32	0.11	0.36	0.36	0.10	0.33	0.22	0.34	0.39	-0.22	0.36	0.18	0.16	-0.52
Car collision speed	0.66	-0.02	0.34	0.68	-0.05	0.36	-0.06	0.44	0.57	0.10	-0.47	0.23	0.56	0.08	-0.70
Impact angle	-0.09	-0.12	0.14	-0.03	0.09	0.28	-0.15	0.25	0.08	0.03	0.11	-0.19	0.21	0.29	0.03
Impact location from car	0.17	0.51	0.10	0.06	-0.06	0.03	-0.04	-0.25	0.15	0.01	-0.09	-0.06	-0.27	-0.06	0.09
Pedaling Posture	-0.08	0.07	0.20	0.04	-0.10	0.14	-0.18	-0.14	0.13	-0.16	-0.02	-0.26	-0.12	-0.07	-0.08
Type of car	0.25	-0.09	0.09	0.23	-0.36	0.02	-0.26	-0.30	0.31	-0.30	-0.21	-0.31	-0.30	-0.45	0.00

Fig. C1. Correlation map with correlations above 0.3 marked in orange for deeper analysis.

- Correlation factor = 0.70
- **Increasing non-linear trend** between car collision speed and X coordination of the head impact.
- Significant scatter in the data show influence of other variables.
- **In overall, the bond is very strong.**

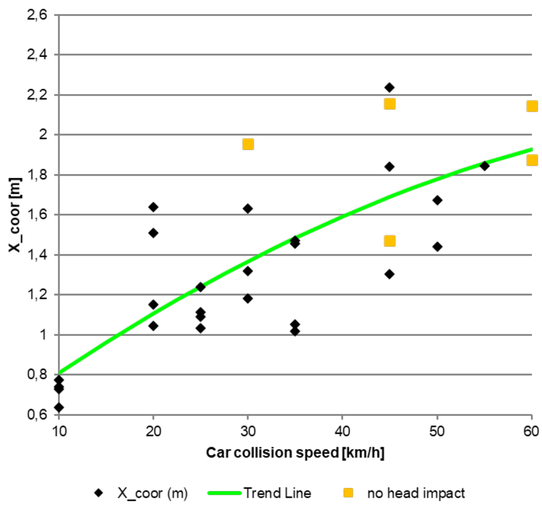

Fig. C2. Example of 2D scatter plot of a variable with high correlation (0.7).

- Correlation factor = 0.37
- **Quadratic non-linear trend** between bicycle collision speed and X coordination of the head impact. Minium of X_coord is in range of 10-15km/h. Clear X_coord growth in higher speeds.
- Value of scatter to "signal" ratio (represented by a trend line) is high. **The bond is weak.**

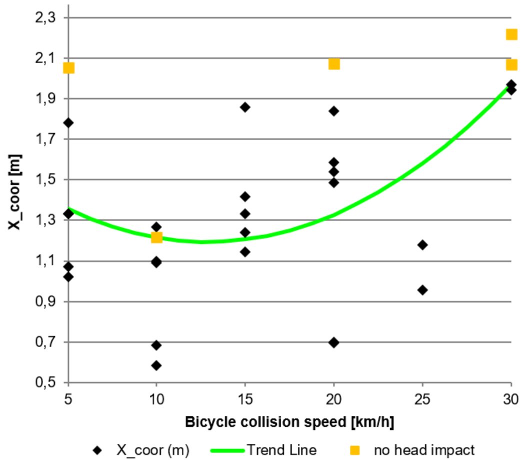

Fig. C3. Example of 2D scatter plot of a variable with low correlation (0.37).

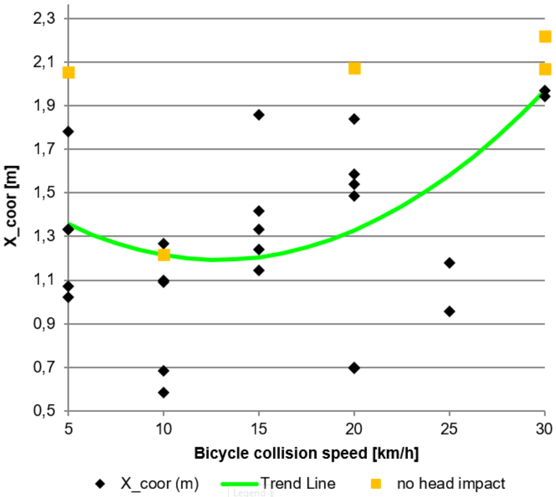
X_coor [m]
Bicycle collision speed [km/h]
X_coor (m)
Trend Line
no head impact

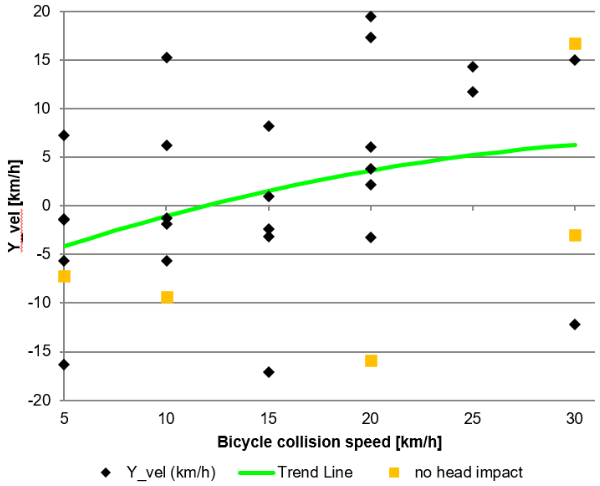
Y_vel [km/h]
Bicycle collision speed [km/h]
Y_vel (km/h)
Trend Line
no head impact

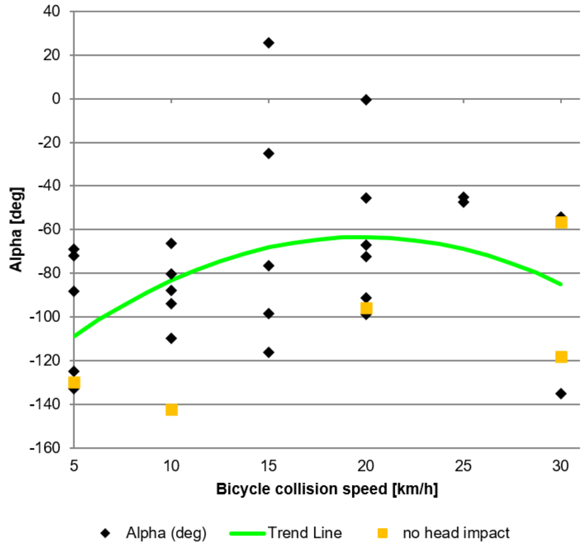
Alpha [deg]
Bicycle collision speed [km/h]
Alpha (deg)
Trend Line
no head impact

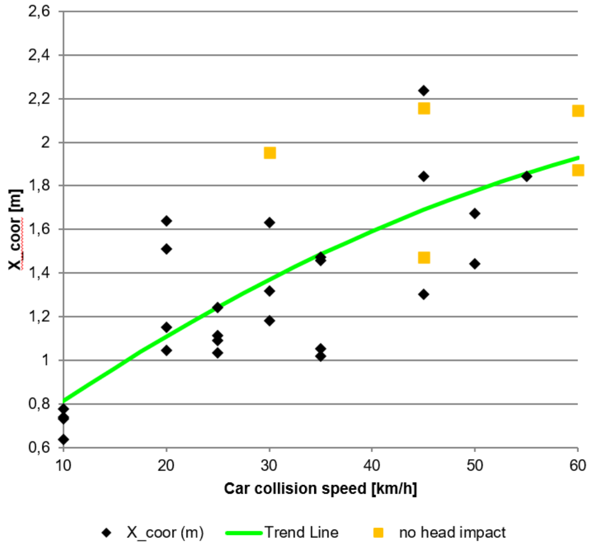
X_coor [m]
Car collision speed [km/h]
X_coor (m)
Trend Line
no head impact

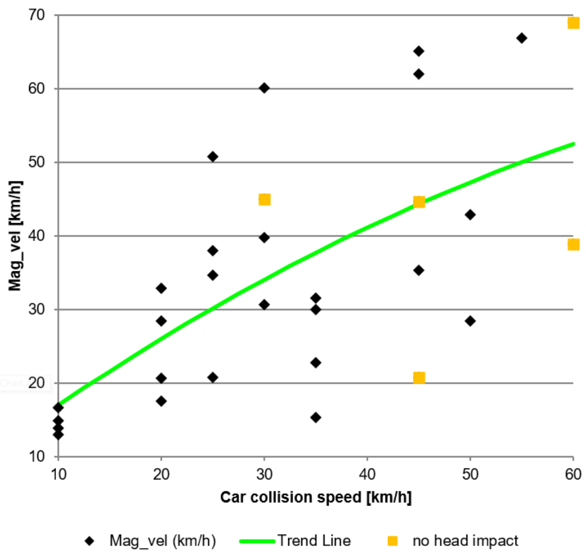
Mag_vel [km/h]
Car collision speed [km/h]
Mag_vel (km/h)
Trend Line
no head impact

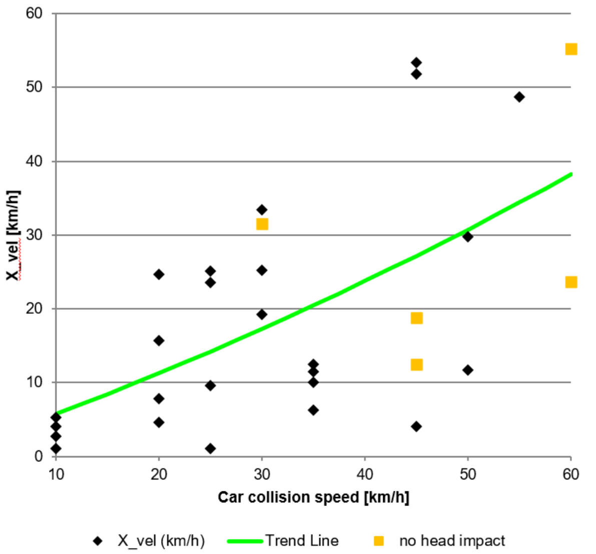
X_vel [km/h]
Car collision speed [km/h]
X_vel (km/h)
Trend Line
no head impact

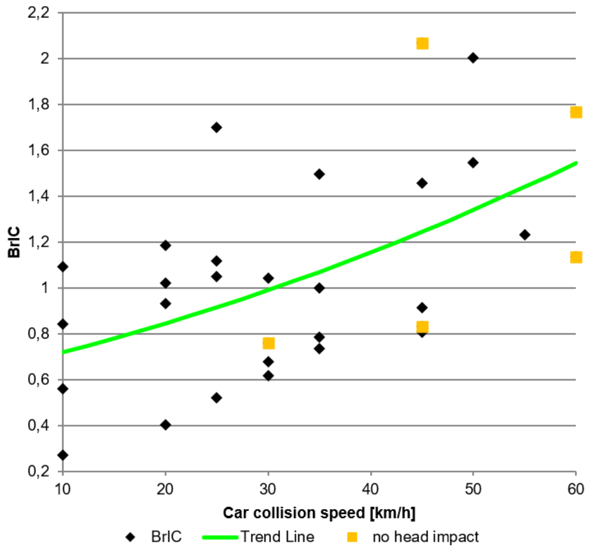
BrIC
Car collision speed [km/h]
BrIC
Trend Line
no head impact

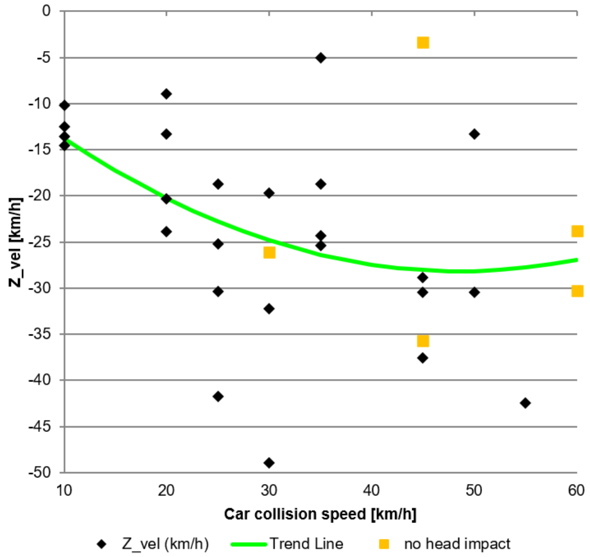
Z_vel [km/h]
Car collision speed [km/h]
Z_vel (km/h)
Trend Line
no head impact

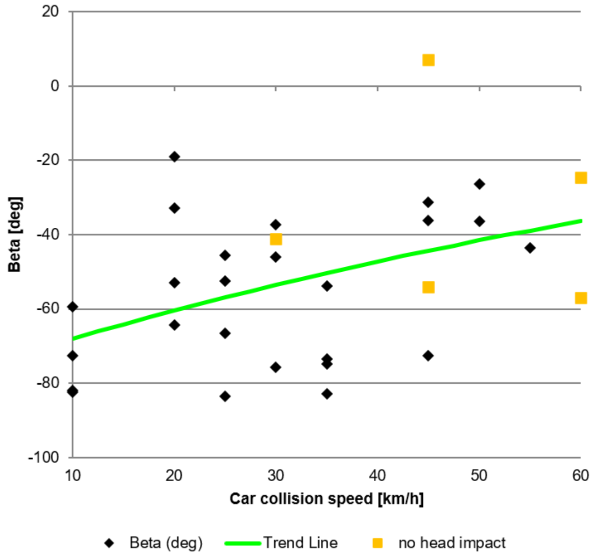
Beta [deg]
Car collision speed [km/h]
Beta (deg)
Trend Line
no head impact

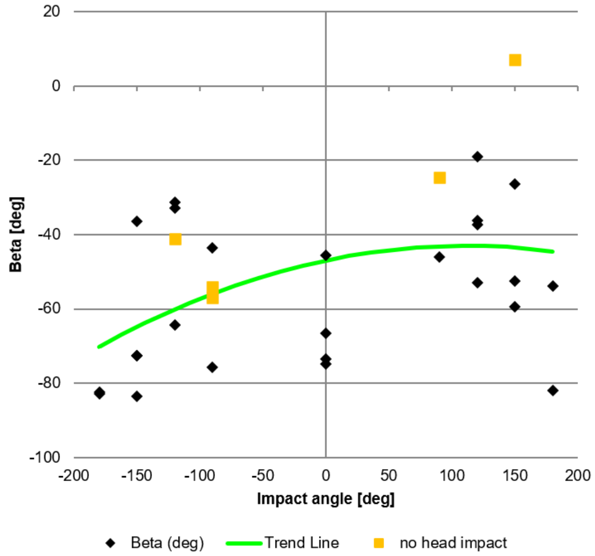
Beta [deg]
Impact angle [deg]
Beta (deg)
Trend Line
no head impact

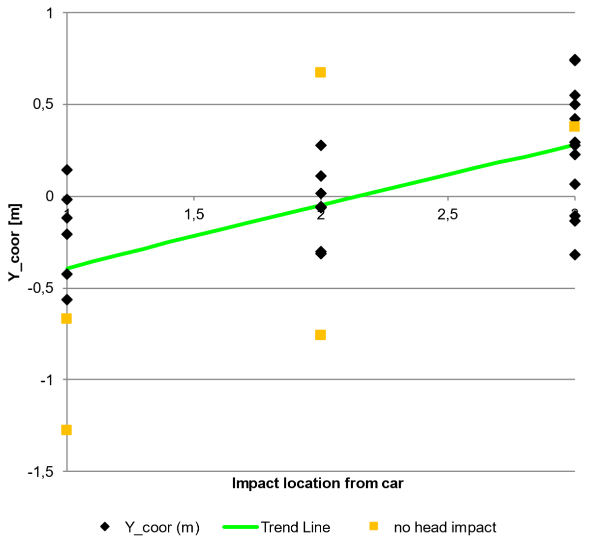
Y_coor [m]
Impact location from car
Y_coor (m)
Trend Line
no head impact

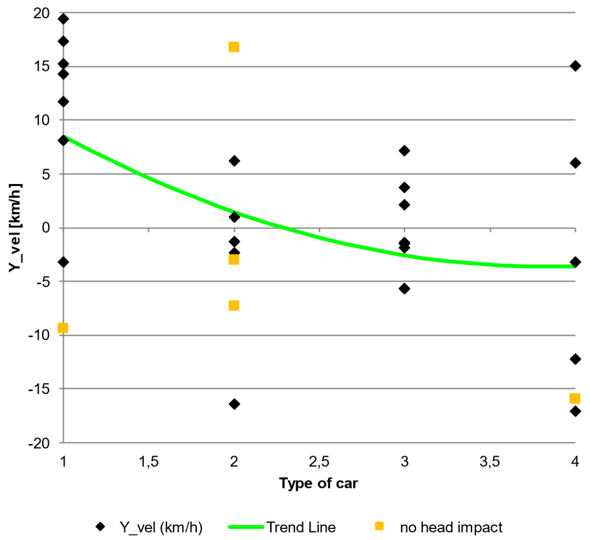
Y_vel [km/h]
Type of car
Y_vel (km/h)
Trend Line
no head impact

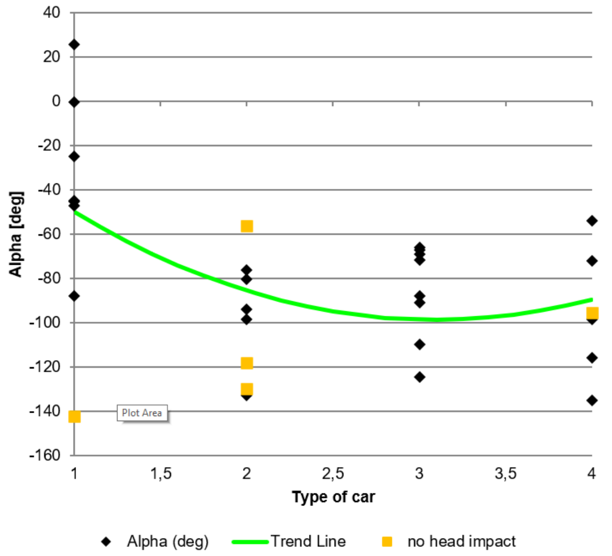
Alpha [deg]
Type of car
Plot Area
Alpha (deg)
Trend Line
no head impact

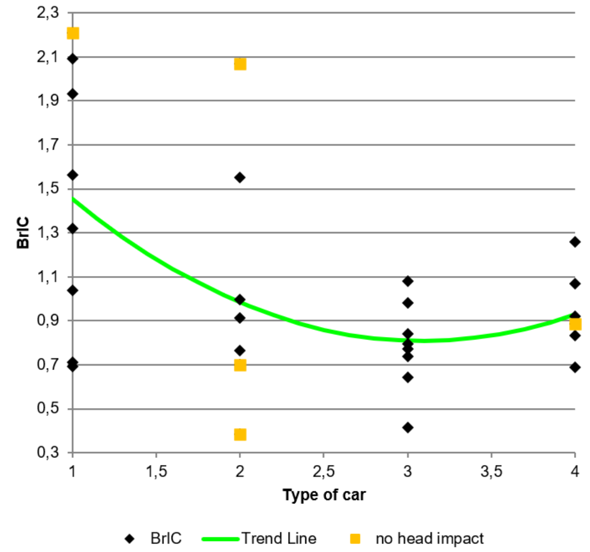
BrIC
Type of car
BrIC
Trend Line
no head impact

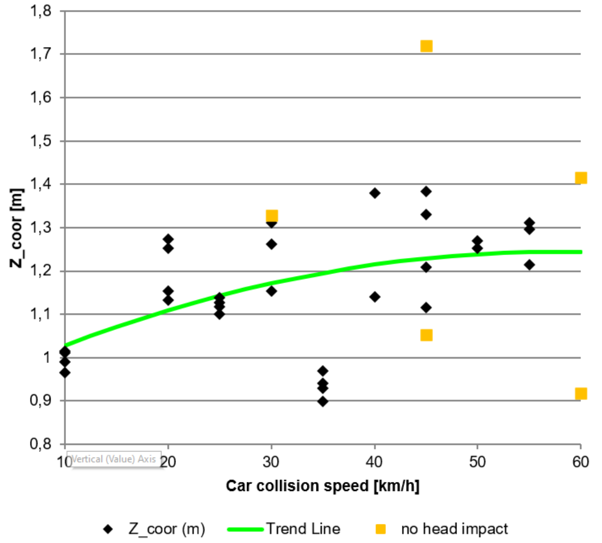
Z_coor [m]
Car collision speed [km/h]
Vertical (Value) Axis
Z_coor (m)
Trend Line
no head impact

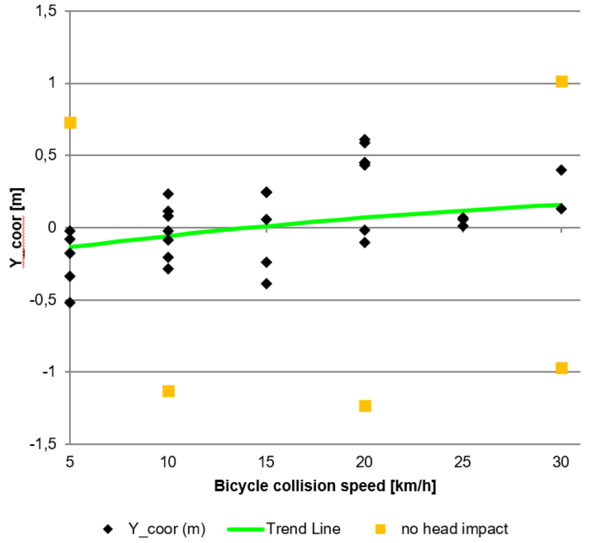
Y_coor [m]
Bicycle collision speed [km/h]
Y_coor (m)
Trend Line
no head impact

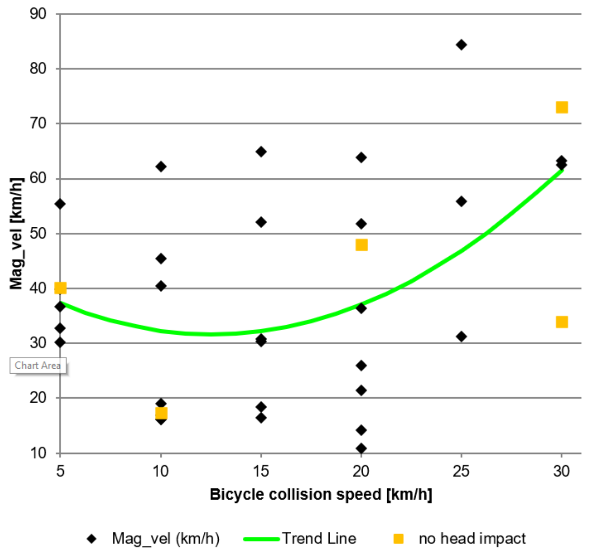
Mag_vel [km/h]
Bicycle collision speed [km/h]
Chart Area
Mag_vel (km/h)
Trend Line
no head impact

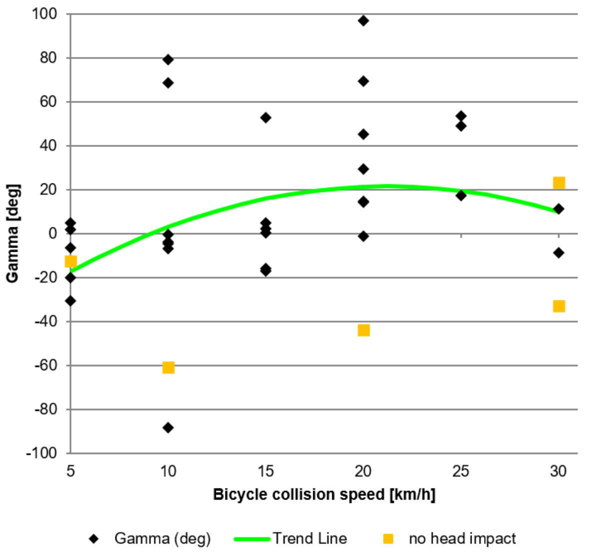
Gamma [deg]
Bicycle collision speed [km/h]
Gamma (deg)
Trend Line
no head impact

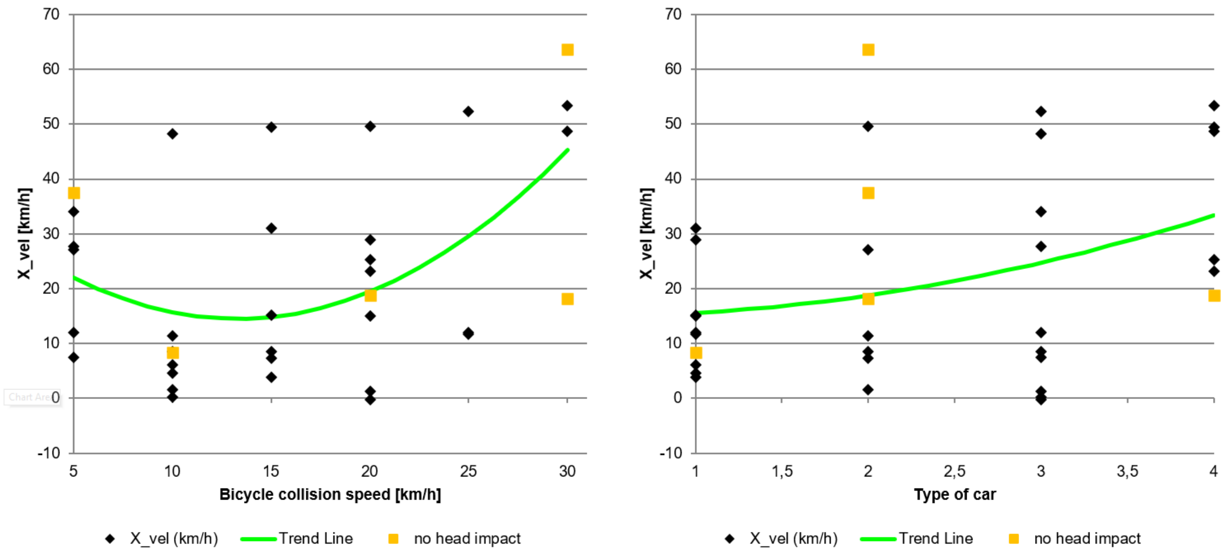

Fig. C4. 2D scatter plots of all the variable combinations with correlation values higher than 0.3 from the study.

Error Analysis Metrics

The following description shows the different metrics that were used in the error analysis to calibrate each RSM.

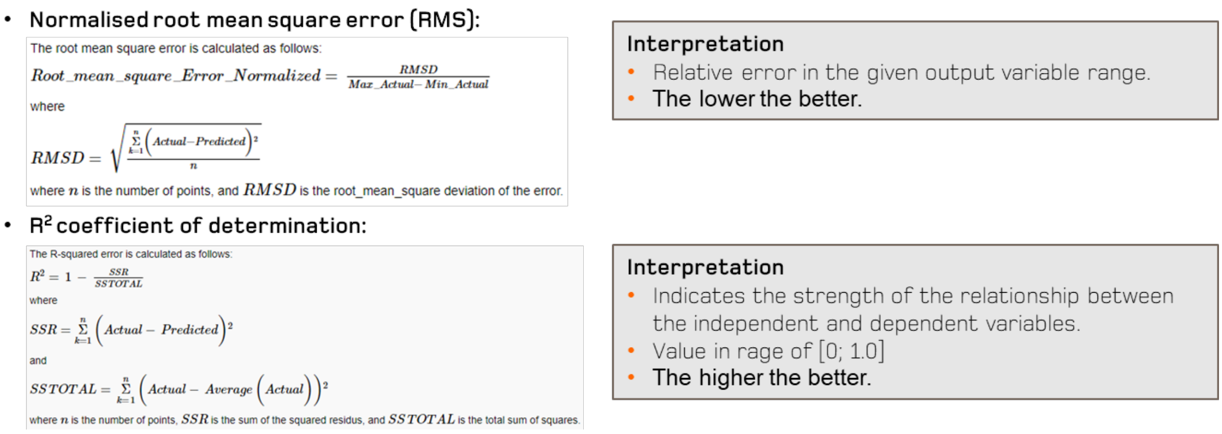

Fig. C5. Error metrics used to perform the error analysis. On the left, the mathematical description of each error metric is shown. On the right is the interpretation of each metric.

Although R^2 is easy to interpret, it overestimates the fit when unnecessary predictors (input variables) are used, especially in models with many input variables and a small number of samples. R^2 can be adjusted to decrease the risk of surrogate model overfitting (i.e., when a new input variable is added) the unadjusted R^2 will not grow unrealistically. Adjusted R^2 can underestimate the true performance of a surrogate model so it can be understood as a more conservative metric but not necessarily more accurate. Adjusted R^2 was calculated with the following formula.

$$R^2 = 1 - \frac{(1 - R^2)(n - 1)}{(n - k - 1)} \tag{C1}$$

Where n is the number of samples and k is the number of input variables.

Response Surface Models

The response surface models obtained in this study are presented in the following tables. Table C I shows the acronyms used for each input parameter of the response surface models.

TABLE C I – ACRONYMS USED FOR EACH INPUT PARAMETER

ACRONYM	INPUT PARAMETER
X01	Bicycle collision speed [km/h]
X02	Car collision speed [km/h]
X03	Impact angle [deg]
X04	Impact location in the car [1=Left, 2=Mid, 3= Right]
X05	Type of car [1=SUV, 2=RDS, 3=MPV, 4=FCR]
X06	Pedaling posture [1=PP1, 2=PP2, 3=PP3, 4=PP4]

Each pedalling posture is shown in Figures C5 to C8.

Fig. C5. Pedaling posture 1 (PP1). Struck-side pedal at bottom dead point. Struck-side leg marked in red.

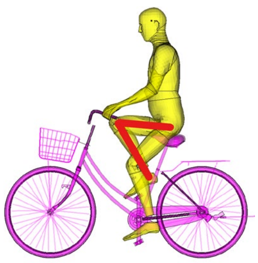

Fig. C6. Pedaling posture 2 (PP2). Struck-side pedal at top dead point. Struck-side leg marked in red.

Fig. C7. Pedaling posture 3 (PP3). Struck-side pedal forward. Struck-side leg marked in red.

Fig. C8. Pedaling posture 4 (PP4). Struck-side pedal backward. Struck-side leg marked in red.

TABLE C II – RESPONSE SURFACE MODEL FOR HEAD X COORDINATE

POLYNOMIAL TERM	COEFFICIENT
Constant	2.4239935236388
X04	-1.48601500819901
X05	-0.681933174341273
X06	0.358585804719216
$X01^2$	0.0029885758760637
$X03^2$	-1.15960758133846e-05
$X04^2$	0.432317734195268
$X05^2$	0.122574868918812
X01*X04	-0.0303218150958951
X01*X05	-0.0121176089574732
X02*X05	0.00875089099578137
X04*X05	0.149528675306126
X04*X06	-0.0516347217511137
X05*X06	-0.104612816880059

TABLE C III – RESPONSE SURFACE MODEL FOR HEAD Y COORDINATE

POLYNOMIAL TERM	**COEFFICIENT**
Constant	0.715215047002264
X03	-0.00540362048781722
X04	0.46295642288209
X06	-0.739441290568352
$X01^2$	-0.00376431264500239
$X02^2$	-0.00122082084417007
X01*X02	0.00426157691468665
X01*X03	0.000309111924404317
X02*X04	-0.0107633878981076
X02*X05	-0.00851854953345588
X02*X06	0.0173875284732135
X03*X04	-0.00112366227223251
X03*X05	0.00123501363876321
X05*X06	0.0797273804436706

TABLE C IV – RESPONSE SURFACE MODEL FOR HEAD Z COORDINATE

POLYNOMIAL TERM	**COEFFICIENT**
Constant	3.07989203558133
X01	-0.030726918327156
X02	-0.0236388583369726
X03	0.000712318852905605
X05	-0.470532285469779
X06	-0.489221037239911
$X04^2$	-0.110095031406307
$X05^2$	0.061445513453738
X01*X02	0.000577277480584363
X02*X03	3.18357089319152e-05
X02*X06	0.00673357297696883
X03*X06	-0.000525978813129221
X04*X05	0.0805506978595547
X04*X06	0.0986601558257578

TABLE C V – RESPONSE SURFACE MODEL FOR HEAD X VELOCITY

POLYNOMIAL TERM	COEFFICIENT
Constant	-17.1724102831316
X01	1.61961287710502
X05	41.4440152759245
X06	-27.8049548057714
$X02^2$	-0.0161847379340803
$X04^2$	-13.9003930151064
$X05^2$	-9.91334669677675
X01*X03	0.0014935671534378
X01*X05	-0.488235172534372
X02*X05	0.309304809396776
X02*X06	0.483050534069462
X04*X05	12.3277180137515
X04*X06	12.6439271709963
X05*X06	-5.94145132556948

TABLE C VI – RESPONSE SURFACE MODEL FOR HEAD Y VELOCITY

POLYNOMIAL TERM	COEFFICIENT
Constant	-38.3230492170556
X01	0.981631840475703
X02	0.978625255350376
X03	-0.201492795503802
X05	11.9226388990451
$X02^2$	-0.00904545541976055
$X03^2$	0.000155985369124883
$X06^2$	-1.23710723565223
X01*X03	0.00431025518696093
X01*X05	-0.534378656910326
X01*X06	0.385958499762926
X02*X03	0.00157592424569639
X02*X05	-0.146526923120788
X03*X05	0.0320961864920576

TABLE C VII – RESPONSE SURFACE MODEL FOR HEAD Z VELOCITY

POLYNOMIAL TERM	COEFFICIENT
Constant	129.606941797035
X01	-2.94542191138675
X02	-2.93758989843832
X04	-54.3405981952493
X05	-43.7498828145899
X06	15.9490545593793
$X02^2$	0.0182044934974707
$X04^2$	17.3719472090816
$X05^2$	6.80909207817179
X01*X02	0.0726761295832944
X03*X04	-0.0226064383532987
X03*X06	0.0239380959851273
X04*X06	-8.05796396144938
X05*X06	2.02917752189232

TABLE C VIII – RESPONSE SURFACE MODEL FOR HEAD MAGNITUDE OF VELOCITY

POLYNOMIAL TERM	COEFFICIENT
Constant	-73.4921584741036
X02	2.73569554794344
X04	81.8606765222261
X05	36.730700856515
X06	-47.4827073456927
$X02^2$	-0.0305823280965082
$X04^2$	-21.513973707482
$X05^2$	-6.55238536557485
X01*X03	0.00508891264560782
X01*X06	0.268733756258467
X02*X04	-0.563791455342465
X02*X06	0.495417823943562
X03*X06	-0.0288824522203182
X04*X06	10.9682124291526

TABLE C IX – RESPONSE SURFACE MODEL FOR HEAD ALPHA ANGLE

POLYNOMIAL TERM	COEFFICIENT
Constant	249.355941542726
X02	-12.0758830074039
X03	-0.565733599944974
X05	-44.9915171299711
$X01^2$	-0.46365617687254
$X04^2$	-15.983099358044
$X06^2$	-3.7886251078823
X01*X02	0.325156055374985
X01*X03	0.0170349279903747
X01*X04	2.18709347577203
X02*X04	0.879886914935274
X02*X05	0.815269450475036
X02*X06	0.636075059287234
X03*X06	0.123855572417231

TABLE C X – RESPONSE SURFACE MODEL FOR HEAD BETA ANGLE

POLYNOMIAL TERM	COEFFICIENT
Constant	43.60224860291
X01	2.16738053770229
X02	-1.34715428667771
X03	0.27700977527424
X04	-87.2401760376478
X05	-20.7753298926658
X01*X05	-1.16819150003503
X02*X04	0.525730561492438
X02*X05	0.468580319432193
X03*X04	-0.0256178533669563
X03*X05	-0.0663848166424618
X04*X05	22.0661869368546
X04*X06	10.218877442537
X05*X06	-8.56308608247621

TABLE C XI – RESPONSE SURFACE MODEL FOR HEAD GAMMA ANGLE

POLYNOMIAL TERM	COEFFICIENT
Constant	-193.629980287944
X01	7.11680632719906
X03	-0.696175171555401
X05	45.6200495816067
X06	94.9257868288795
$X03^2$	0.00135654875817963
$X04^2$	-10.3911159087493
$X05^2$	-9.74219743406107
$X06^2$	-19.9942361489166
X01*X02	-0.15865819294113
X01*X03	0.0119791396760718
X02*X03	0.00447704784275391
X02*X04	1.19877431238938
X03*X05	0.0458309862346981